The Radiated Seismic Energy and Apparent Stress of Interplate and Intraplate Earthquakes at Subduction Zone Environments: Implications for Seismic Hazard Estimation

by George L. Choy[1]
John L. Boatwright[2]
Steve Kirby[2]

Open-File Report 01-0005

2001

U.S. DEPARTMENT OF THE INTERIOR
U.S. GEOLOGICAL SURVEY

[1]Denver, Colorado
[2]Menlo Park, California

The Radiated Seismic Energy and Apparent Stress of Interplate and Intraslab Earthquakes at Subduction Zone Environments: Implications for Seismic Hazard Estimation

George L. Choy, U. S. Geological Survey, Golden, CO
John L. Boatwright, U. S. Geological Survey, Menlo Park, CA
Steve Kirby, U. S. Geological Survey, Menlo Park, CA

Abstract. The radiated seismic energies (E_S) of 980 shallow subduction-zone earthquakes with magnitudes ≥ 5.8 are used to examine global patterns of energy release and apparent stress. In contrast to traditional methods which have relied upon empirical formulas, these energies are computed through direct spectral analysis of broadband seismic waveforms. Energy gives a physically different measure of earthquake size than moment. Moment, being derived from the low-frequency asymptote of the displacement spectra, is related to the final static displacement. Thus, moment is crucial to the long-term tectonic implication of an earthquake. In contrast, energy, being derived from the velocity power spectra, is more a measure of seismic potential for damage to anthropogenic structures. There is considerable scatter in the plot of E_S-M_0 for worldwide earthquakes. For any given M_0, the E_S can vary by as much as an order of magnitude about the mean regression line. The global variation between E_S and M_0, while large, is not random. When subsets of E_S-M_0 are plotted as a function of seismic region, tectonic setting and faulting type, the scatter in data is often substantially reduced. There are two profound implications for the estimation of seismic and tsunamic hazard. First, it is now feasible to characterize the apparent stress for particular regions. Second, a given M_0 does not have a unique E_S. This means that M_0 alone is not sufficient to describe all aspects of an earthquake. In particular, we have found examples of interplate thrust-faulting earthquakes and intraslab normal-faulting earthquakes occurring in the same epicentral region with vastly different macroseismic effects. Despite the gross macroseismic disparities, the M_W's in these examples were identical. However, the M_e's (energy magnitudes) successfully distinguished the earthquakes that were more damaging.

Introduction

There are two compelling reasons for using radiated seismic energy as a complement to moment in estimating seismic and tsunamic hazard. First, energy gives a physically different measure of earthquake size than moment. Energy is derived from the velocity power spectra, while moment is derived from the low-frequency asymptote of the displacement spectra. Thus, moment, being related to the final static displacement, is crucial to the long-term tectonic implication of an earthquake. In contrast, energy, being strongly peaked about the corner frequency of an earthquake, is more a measure of seismic potential for damage to anthropogenic structures. Secondly, significant regional and tectonic variations in energy release are suppressed by empirical formulas. Choy and Boatwright (1995) demonstrated that systematic variations in the release of energy and in apparent stress can now be identified that were previously undetectable because of the lack of reliable energy estimates. In this paper, we first review some of the important findings from Choy and Boatwright (1995) and then proceed to identify classes of

earthquakes with unusually high intensity of energy release relative to moment release. In particular, there is a substantial difference in the energy radiated by normal-faulting intraslab earthquakes and by thrust-faulting interplate earthquakes. Although M_0 (or its derived magnitude M_W) can characterize the area affected by the rupture, E_S (or its derived magnitude M_e) is more capable of describing macroseismic effects. Also, the highest apparent stresses of any earthquake group are associated with strike-slip faulting earthquakes occurring in oceanic environments. Contrary to conventional wisdom, many of these oceanic strike-slip earthquakes have been associated with tsunamis.

Previous methods of computing radiated seismic energy, E_S:

The computation of the seismic energy radiated by an earthquake simply requires an integration of radiated energy flux in velocity-squared seismograms. However, most methods of computing energy have historically relied on empirical formulas because routine spectral analysis was impractical with analog data. Two common methods use the Gutenberg-Richter formulas which derive E_S from a magnitude

$$log\ E_S = 5.8 + 2.4\ m_b$$
$$log\ E_S = 11.8 + 1.5\ M_S$$

(in units of dyne·cm). More recently, it has been suggested that

$$E_S \sim 5 \times 10^{-5}\ M_0.$$

Notice that in all these formulas that E_S is never actually computed . Instead it is predicated on another value (m_b, M_S or M_0). No new information is really obtained about the earthquake.

Direct measurement of radiated seismic energy:

Fortunately, theoretical and technological impediments to the direct computation of radiated energy have now been removed. The requisite spectral bandwidth is now recorded digitally by a number of seismograph networks and arrays with broadband capability. In addition, corrections for source mechanism and frequency-dependent wave propagation are better understood now than at the time empirical formulas were first developed. We briefly describe the method of Boatwright and Choy (1986).

For shallow earthquakes where the source functions of direct and surface-reflected body-wave arrivals may overlap in time, the radiated energy of a *P*-wave group (consisting of *P*, *pP* and *sP*) is related to the energy flux by

$$E_S^P = 4\pi\ <F^P>^2 \left(\frac{R^P}{F^{gP}}\right)^2 \varepsilon_{gP}^*$$

where the P-wave energy flux, ε_{gP}^*, is the integral of the square of the ground velocity,

corrected for frequency-dependent attenuation; $<F^P>^2$ is the mean-square radiation-pattern coefficient for P waves; R^P is the P-wave geometrical spreading factor; F^{gP} is the generalized radiation pattern coefficient for the P-wave group defined as

$$\left(F^{gP}\right)^2 = \left(F^{P}\right)^2 + \left(\hat{PP}\ \ F^{pP}\right)^2 + \frac{2\alpha q}{3\beta}\left(\hat{SP}\ \ F^{sP}\right)^2$$

where F^i are the radiation-pattern coefficients for $i = P$, pP, and sP; $\hat{PP}$ and $\hat{SP}$ are plane-wave reflection coefficients of pP and sP at the free surface, respectively, and corrected for free-surface amplification at the receiver; and q is ratio of S-wave energy to P-wave energy. The correction factors explicitly take into account our knowledge that the earthquake is a double-couple, that measurements of the waveforms are affected by interference from depth phases, and that energy is partitioned between P and S waves. The total radiated energy when using the P-wave group is $E_s = (1+q)E_s^P$.

Energy magnitude:

From the radiated energies for a set of 378 global shallow earthquakes Choy and Boatwright (1995) defined an energy magnitude, M_e,

$$log\ E_S = 4.4 + 1.5\ M_e$$

or

$$M_e = 2/3\ log\ E_S - 2.9$$

where E_S is in units of Newton·meters. Note that magnitude M_e is derived explicitly from energy (whereas in the Gutenberg-Richter formula energy is derived from magnitude).

Although M_e and M_W are magnitudes that describe the size of an earthquake, they are not equivalent. Because they measure different physical properties of an earthquake, there is no *a priori* reason that they should numerically equal for any given seismic event. Indeed, in the following sections we show that earthquakes with the same M_W can cause different macroseismic effects. While the macroseismic effects cannot be distinguished by M_W, they can be quantified by M_e. The energy magnitude, M_e, is an essential complement to moment magnitude, M_W, for assessing seismic potential.

The energy and moment of an earthquake are related by apparent stress, $\tau_a = \mu\ E_s / M_0$, where μ is the average rigidity at the source. Apparent stress also serves as a good indicator of the intensity of seismic energy radiation, E_S, relative to the size of the event as measured by the seismic moment M_0. A plot of E_s-M_o for the worldwide population of earthquakes exhibits large scatter (Figure 1a). However, when data are separated into subsets based on faulting mechanism and seismic region, the scatter in the E_s-M_o plots can be relatively small. The important point is that no single empirical formula can hope to predict E_S from M_0. Indeed, these differences can be

exploited to detect patterns of energy and moment that were previously masked by empirical formulas.

Systematic variations in energy release and apparent stress

As a function of seismic region and faulting type: The first step in sorting out the scatter in the E_S-M_0 plot is to separate the populations by faulting mechanism. Figure 1a shows the E_S-M_0 plot for the global set of shallow earthquakes with magnitude ≥ 5.8 that have occurred between 1988-1999. Figures 1b-1d show E_S-M_0 for subsets consisting of earthquakes whose focal mechanisms are predominantly thrust, normal and strike-slip faulting mechanisms, respectively. Although the scatter is still large, the geometric spread about the average value of each subset does seem to have been reduced. On a global scale, the average apparent stress of strike-slip faulting earthquakes is much greater than that for normal-faulting earthquakes, which in turn is slightly larger than that for thrust-faulting earthquakes.

If we separate the data into subsets by region and mechanism, or by tectonic setting and mechanism, we find the reduction in the geometric spread is more dramatic (Choy and Boatwright,1995). For most regions of the world the geometric spread is so narrow for a given faulting type that the average apparent stress can be regarded as the characteristic apparent stress (τ_c) of the region. Two examples are shown here (Figures 2a and 2b), for thrust-fault earthquakes at the Aleutian arc and the Chile trench. A preliminary global map of the characteristic apparent stress of thrust-faulting earthquakes for seismic regions is shown in Figure 3. A τ_c was computed for a seismic region only if τ_a's from at least 5 earthquakes were available. A similar mapping of characteristic apparent stress for normal-faulting and strike-slip faulting earthquakes is not yet possible because of the relative paucity of such events. As more statistics on the release of energy are accumulated, spatial and temporal variations in energy release and apparent stress can be refined.

As a function of tectonic setting and faulting type: The geometric spread in the E_S-M_0 plot is also small for subsets based on earthquakes in specific tectonic settings. Figure 4 shows the data for the set of continental intraplate thrust-faulting earthquakes. Note that the average apparent stress for continental intraplate events is greater than the average for subduction-zone thrust-faulting earthquakes.

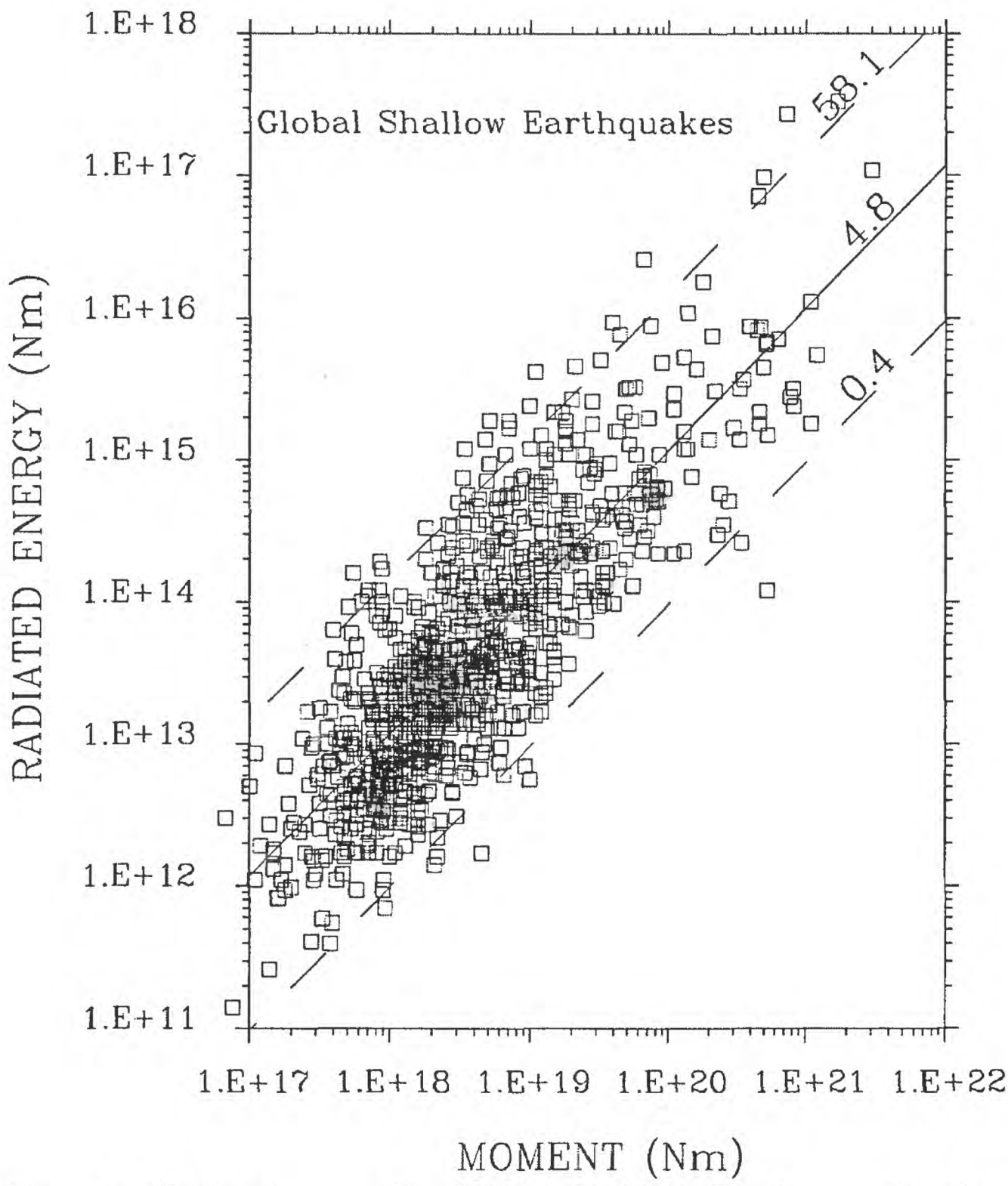

Figure 1a. . Radiated energy (E_S) of 980 worldwide shallow-focus earthquakes that occurred between 1988 to 1999 as a function of moment (M_0). The radiated energies are taken from the Monthly Listings of the PDE (Preliminary Determination of Epicenters) published by the NEIC (National Earthquake Information Center) of the U.S.G.S. The slope of the least-squares linear regression (solid line) yields a global average apparent stress for subduction zone earthquakes of 2.7 bars. The 95% geometric spread (width of distribution) about the regression line is indicated by the dashed lines.

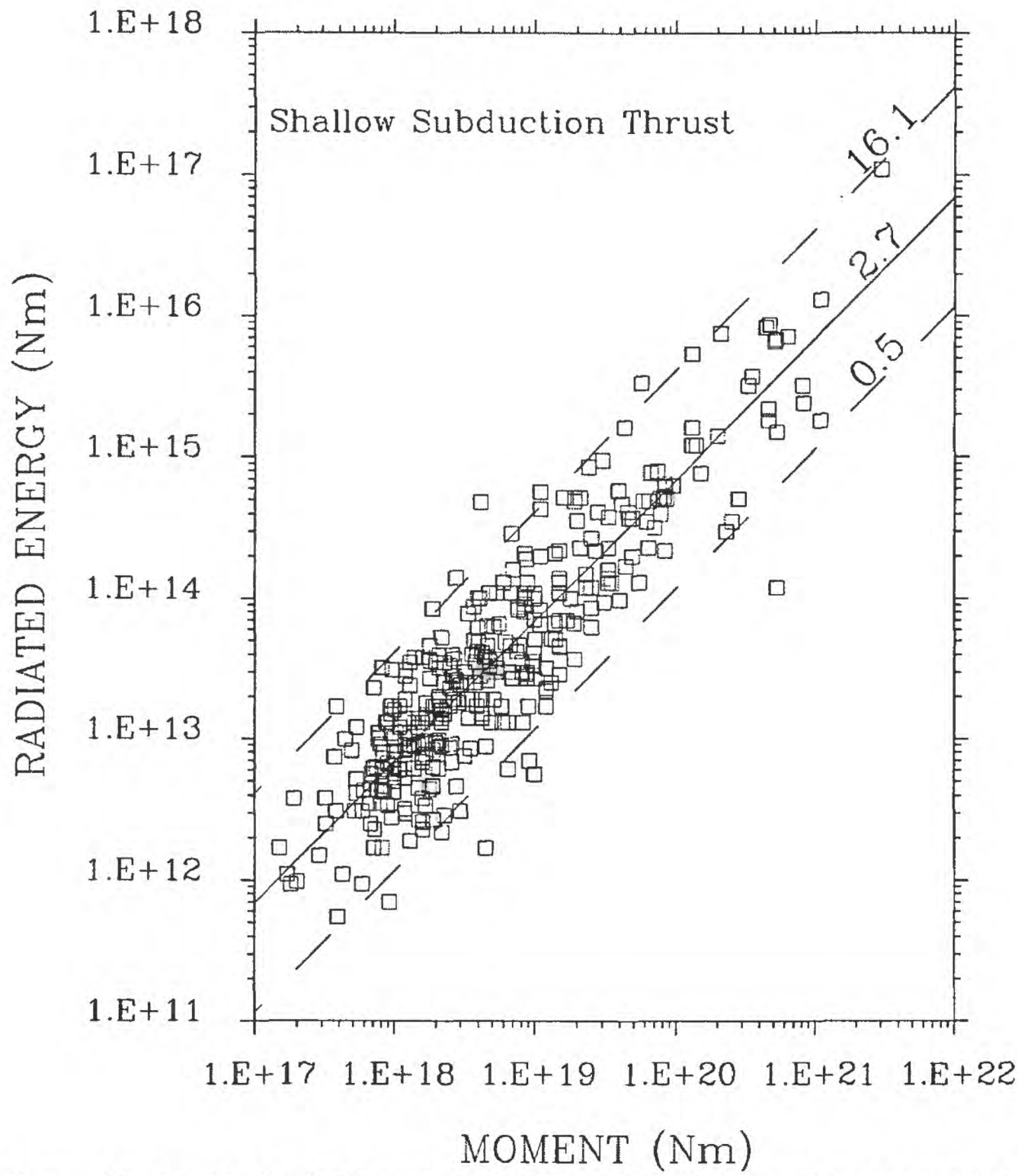

Figure 1b. E_S-M_0 plot for the subset of 355 shallow-focus earthquakes located near subduction zones with predominantly thrust-faulting focal mechanisms. The geometric spread is significantly smaller for this subset than for the set of worldwide earthquakes.

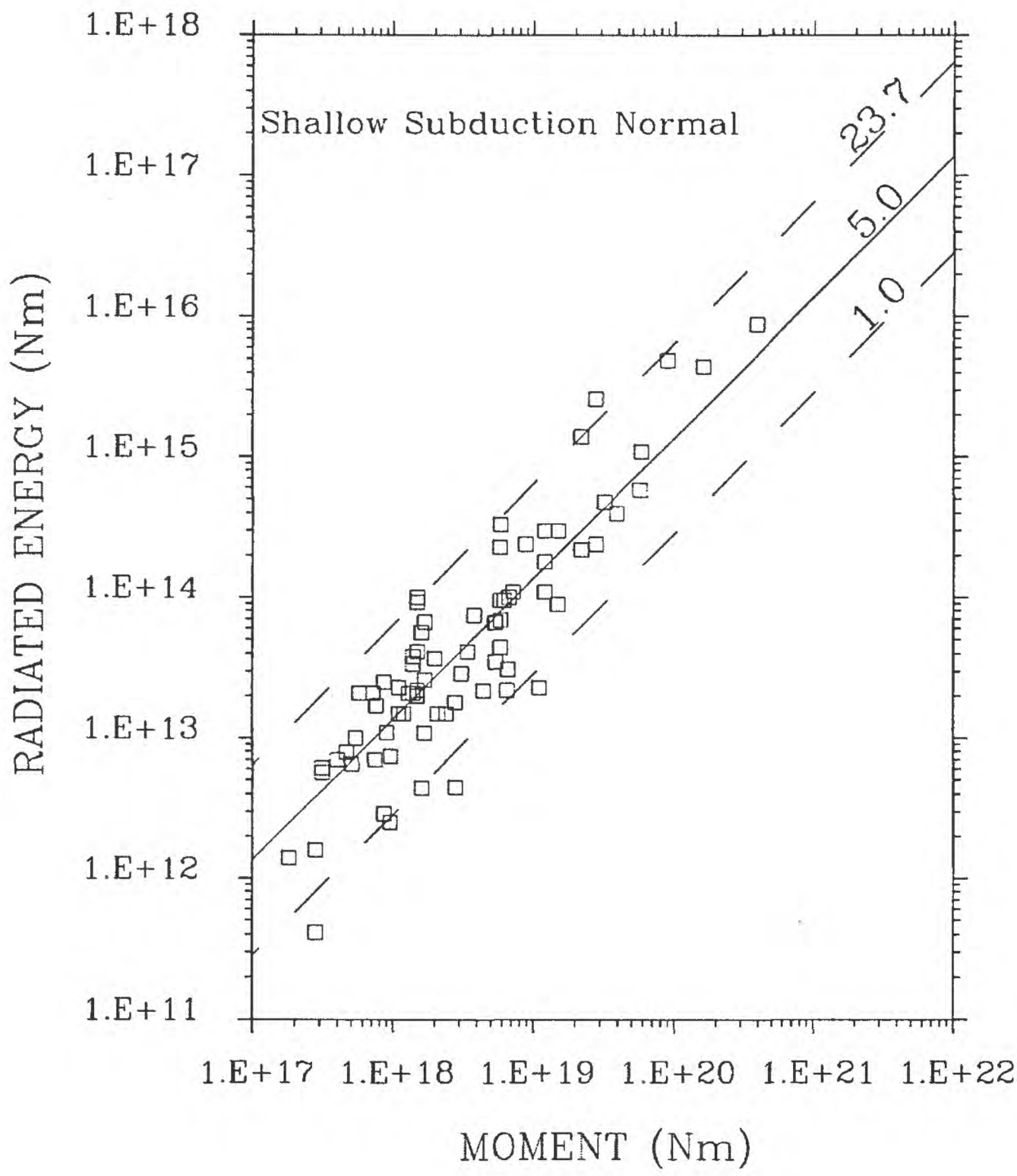

Figure 1c. E_S-M_0 for the subset of 76 shallow-focus earthquakes located near subduction zones with predominantly normal-faulting focal mechanisms. The geometric spread is smaller for this subset than for the set of worldwide earthquakes.

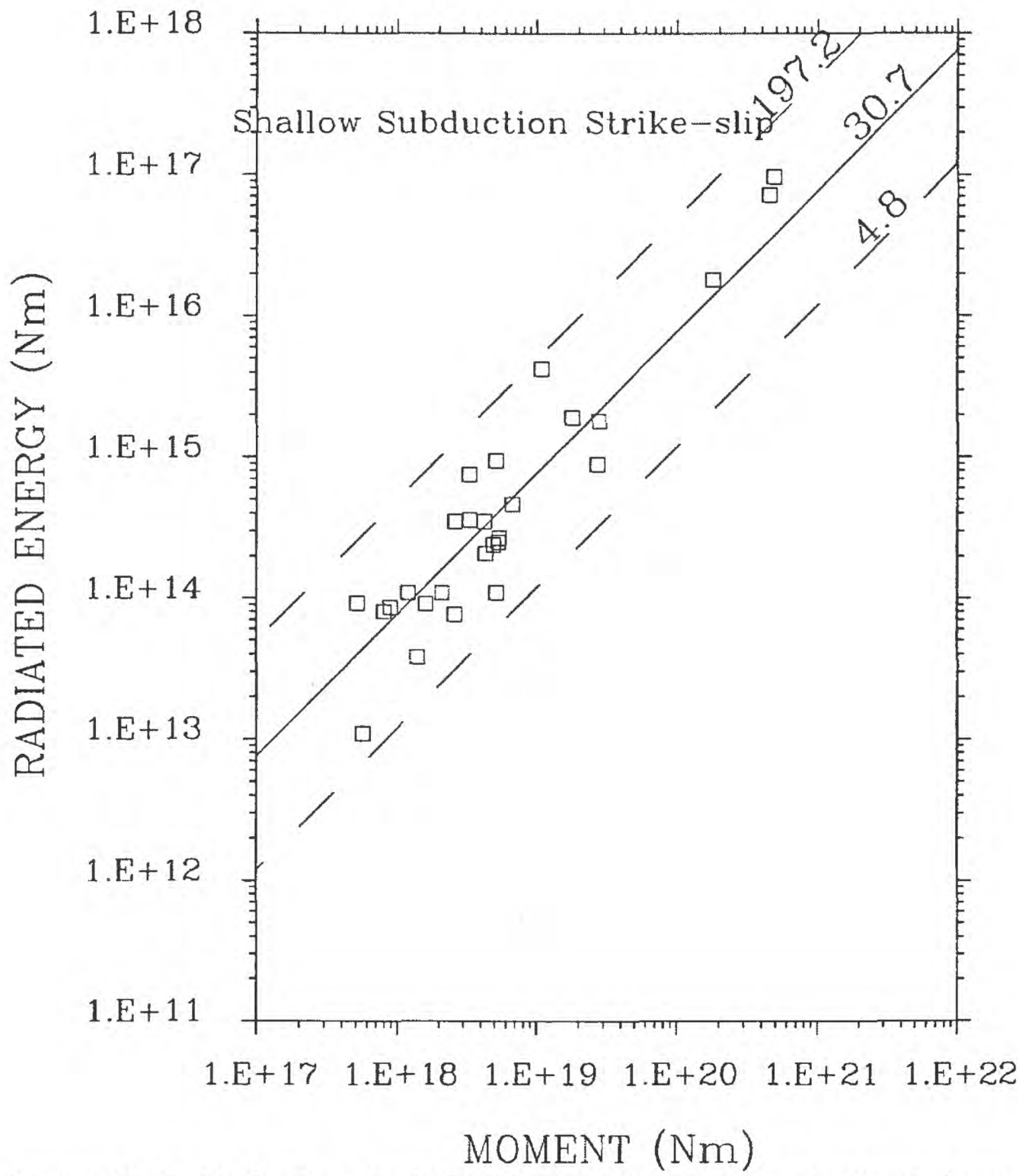

Figure 1d. E_S-M_0 for the subset of 27 shallow-focus earthquakes located near subduction zones with predominantly strike-slip focal mechanisms. The average apparent stress of strike-slip earthquakes is a magnitude larger than that for the earthquakes with dip-slip mechanisms.

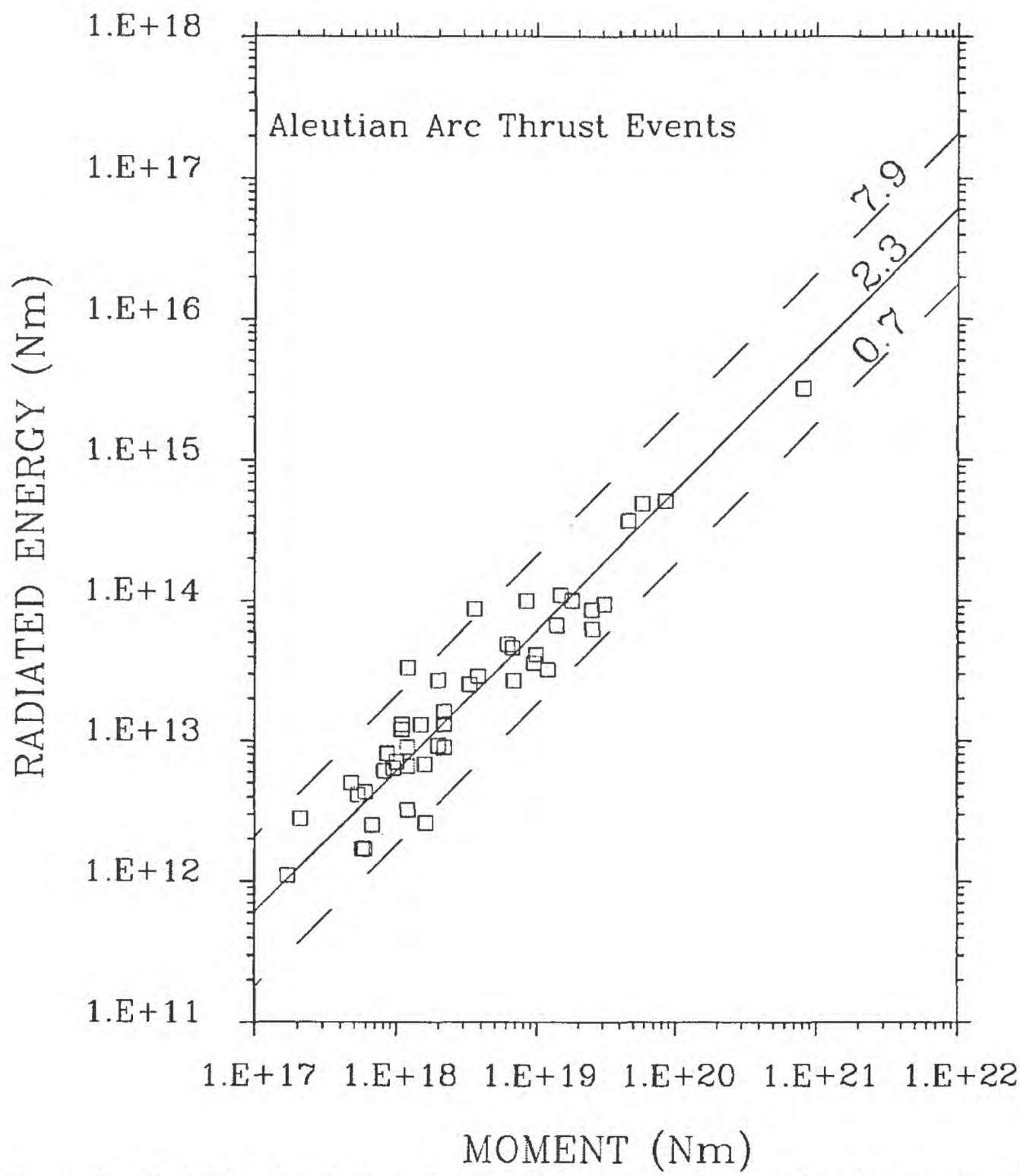

Figure 2a. E_S-M_0 for 46 shallow-focus thrust-faulting earthquakes that occurred between 1988 to 1999 along the Aleutian arc. The characteristic apparent stress for this seismic region is centered narrowly about 2.3 bars.

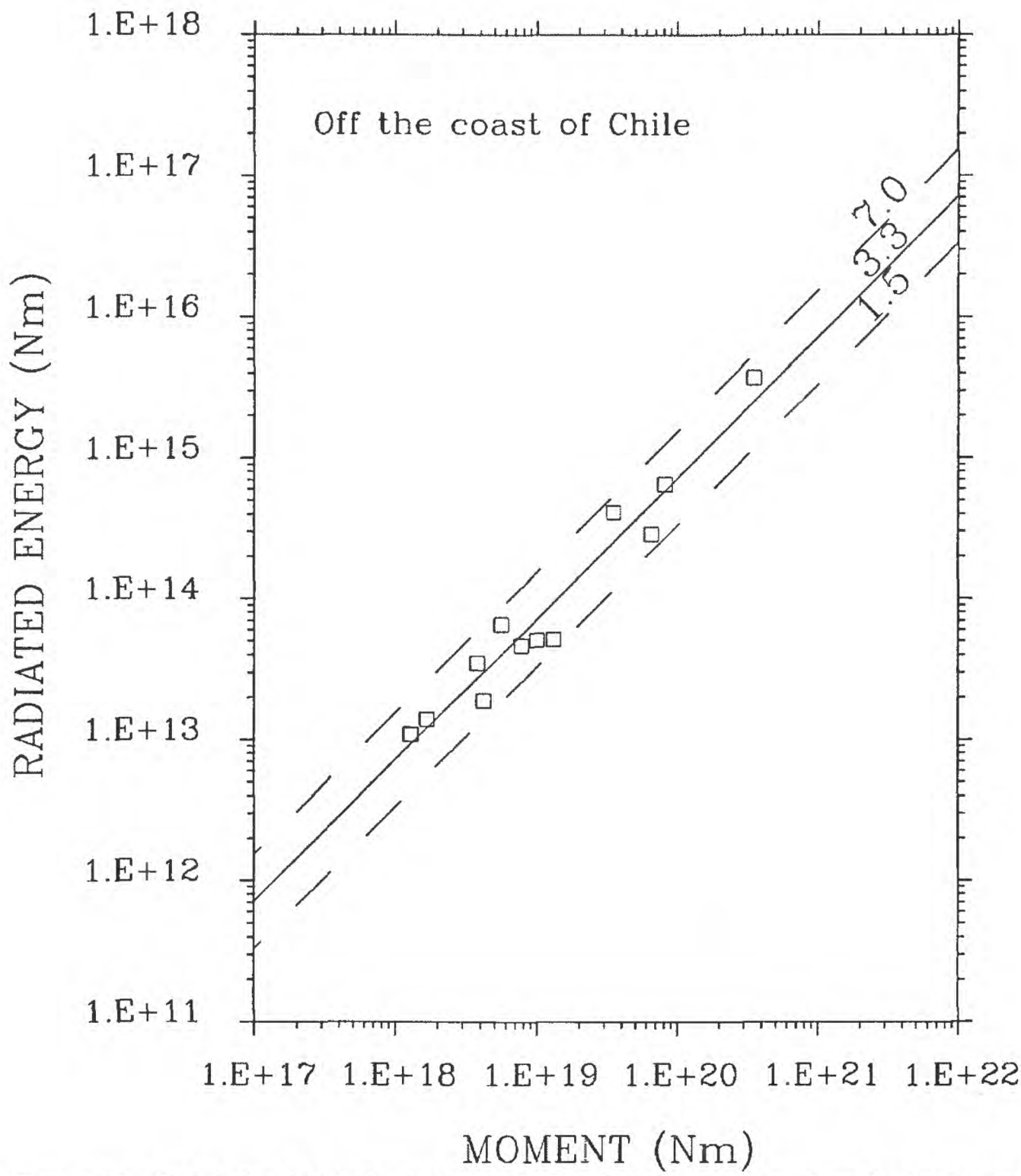

Figure 2b. E_S-M_0 for 12 shallow-focus thrust-faulting earthquakes that occurred between 1988 to 1994 along the Chile trench. The characteristic apparent stress for this seismic region is centered narrowly about 3.3 bars.

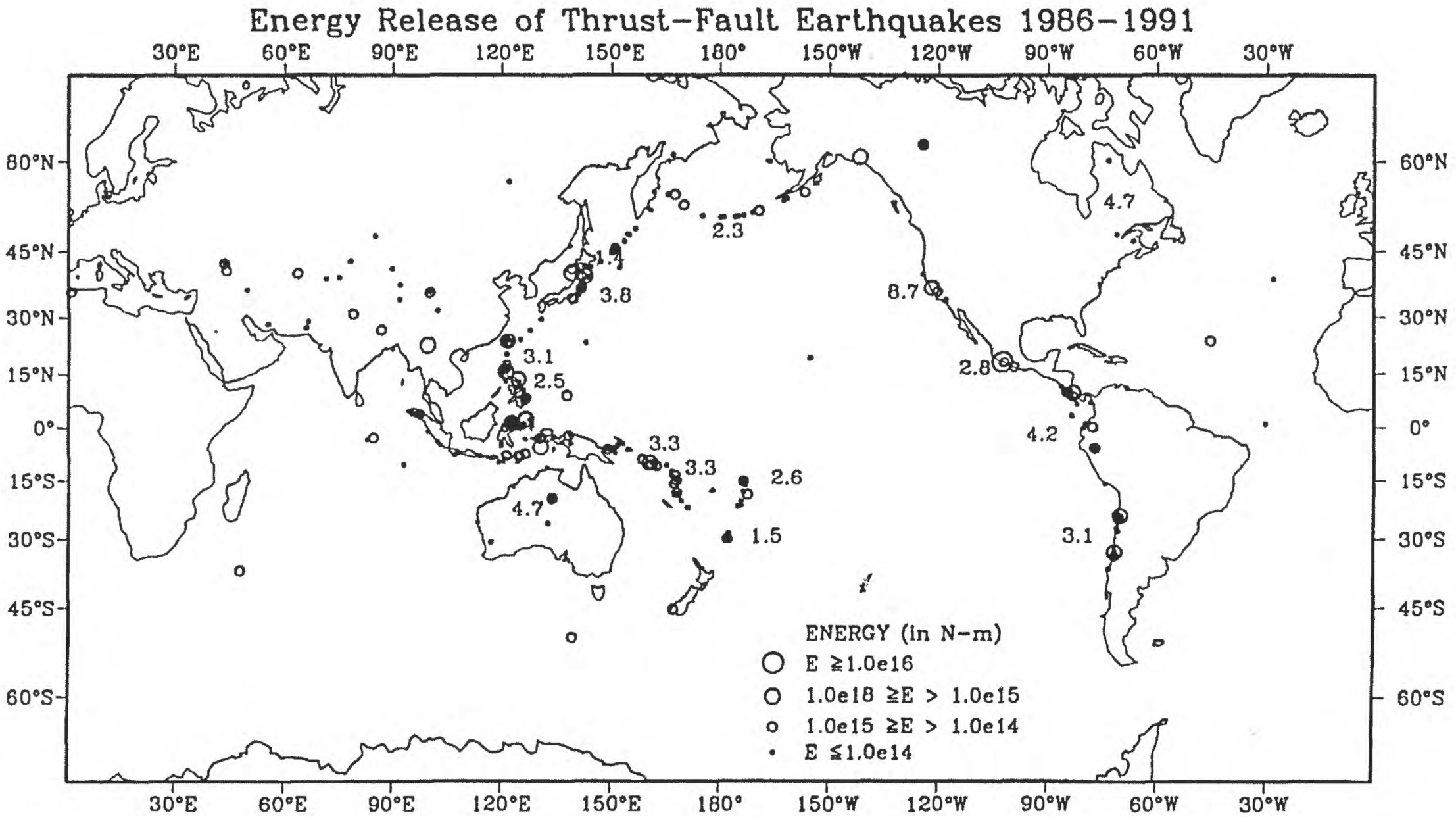

Figure 3. Global patterns of energy release for all large ($E_S > 10^{10}$ N·m) shallow thrust-fault earthquakes that occurred between 1988-1991. The characteristic apparent stress, τ_c, is indicated for those seismic regions where the geometric spread about the average stress in the E_S-M_0 plot is less than 15 bars.

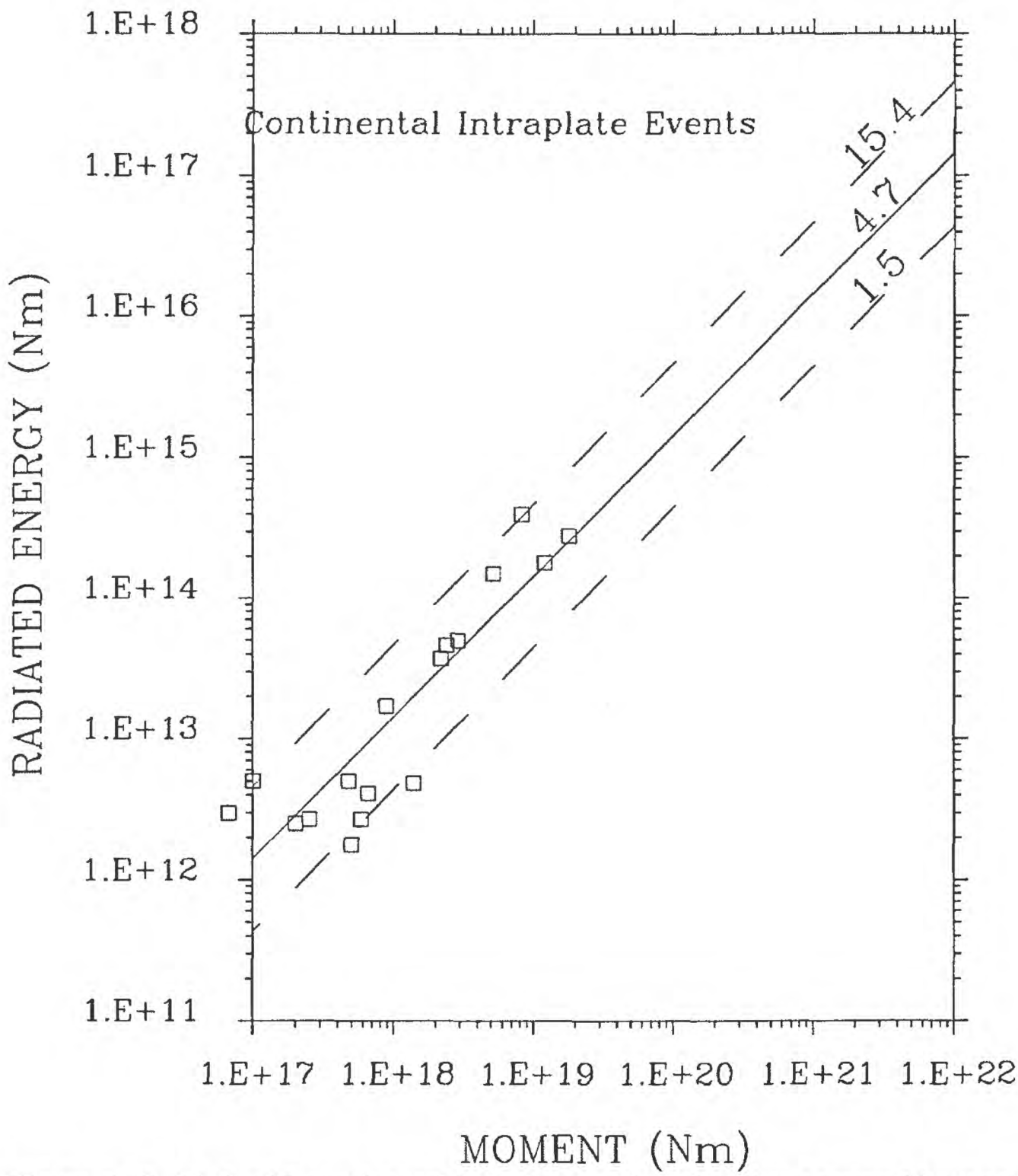

Figure 4. E_S-M_0 for 17 continental intraplate earthquakes that occurred between 1988 to 1999. The characteristic apparent stress for earthquakes in this tectonic setting is centered narrowly about 4.7 bars, which is slightly higher than average for all subduction-zone thrust earthquakes.

Normal-faulting intraslab earthquakes: We found two normal-faulting intraslab earthquakes that occurred in the immediate vicinity of interplate thrust-faulting events. For these two earthquakes we could make a direct comparison of the relative amount of moment and energy associated with the different faulting types and tectonic settings.

The source parameters and macroseismic reports of two events that occurred in Chile are summarized in Table 1. The epicenter of the interplate thrust-faulting event of July 1997 is less than one degree from that of the intraslab normal-faulting event of October 1997. Despite the nearly identical M_S's and M_W's, as well as the spatial and temporal proximity of the epicenters, the intraslab normal-fault event caused extensive damage and loss of life, whereas the effects of the interplate thrust-fault event were minor. M_W is unable to quantify the conspicuous difference in damage reports. On the other hand, the M_e's are commensurate with the disparity in macroseismic effects. The M_e of the intraslab earthquake, which caused much greater damage, is almost one and one-half magnitudes larger than the M_e of the interplate event.

TABLE 1. NEAR THE COAST OF CENTRAL CHILE

Date	LAT (°)	LON (°)	Depth (km)	M_e	M_W	m_b	M_S	τ_a (bars)	Faulting Type
6 JUL 1997 (1)	-30.06	-71.87	23.0	6.1	6.9	5.8	6.5	1	interplate-thrust
15 OCT 1997 (2)	-30.93	-71.22	58.0	7.6	7.1	6.8	6.8	82	intraslab-normal

Notes:

(1) Felt (III) at Coquimbo, La Serena, Ovalle and Vicuna.

(2) Five people killed at Pueblo Nuevo, one person killed at Coquimbo, one person killed at La Chimba and another died of a heart attack at Punitaqui. More than 300 people injured, 5,000 houses destroyed, 5,700 houses severely damaged, another 10,000 houses slightly damaged, numerous power and telephone outages, landslides and rockslides in the epicentral region. Some damage (VII) at La Serena and (VI) at Ovalle. Felt (VI) at Alto del Carmen and Illapel; (V) at Copiapo, Huasco, San Antonio, Santiago and Vallenar; (IV) at Caldera, Chanaral, Rancagua and Tierra Amarilla; (III) at Talca; (II) at Concepcion and Taltal. Felt as far south as Valdivia. Felt (V) in Mendoza and San Juan Provinces, Argentina. Felt in Buenos Aires, Catamarca, Cordoba, Distrito Federal and La Rioja Provinces, Argentina. Also felt in parts of Bolivia and Peru.

Another example of the disparity in damage between interplate and intraplate earthquakes can be seen in a suite of earthquakes that occurred in Kodiak, Alaska (Table 2). Again, although the epicenters and M_W's are similar (particularly between the first and third events), the macroseismic effects associated with the normal-faulting intraslab earthquakes are far greater than those of the interplate thrust-faulting earthquake. The differences in macroseismic effects can not be distinguished if one were to rely solely on differences in M_W, but they are well quantified by the M_e's.

TABLE 2. KODIAK ISLAND REGION OF ALASKA

Date	LAT (°)	LON (°)	Depth (km)	M_e	M_W	m_b	M_S	τ_a (bars)	Faulting Type
MAY 7 1999 (1)	56.42	-152.94	20.0	5.8	6.3	5.7	6.1	2	interplate-thrust
DEC 6 1999(2)	57.41	-154.49	52.0	7.0	7.0	6.8	---	17	intraslab-normal
DEC 7 1999(3)	57.36	-154.1	45.0	6.9	6.5	6.5	6.1	15	intraslab-normal
JUL 11 2000(4)	57.60	-154.51	49.0	6.8	6.7	6.3	6.3	25	intraslab-normal

Notes:
(1) No felt reports.
(2) Slight damage (VI) at Larsen Bay and Old Harbor. Felt strongly at Akhiok and Kodiak. Felt (III) at Homer and Chignik; (II) at Anchorage, Palmer and Willow. Also felt at Dillingham, Eagle River, Fairbanks, Kasilof, Nelson Lagoon and Nikiski.
(3) Felt at Anchorage, Ekwok, Homer, King Salmon, Kodiak and Old Harbor.
(4) Some minor damage on Kodiak. Felt throughout southern Alaska and as far north as Fairbanks.

The relative paucity of normal-faulting events precludes a similar comparison for most seismic regions. Nevertheless, radiated energy, apparent stress and M_e are clearly valuable considerations in evaluating seismic hazard.

Tsunamic Potential:

Choy and Boatwright (1995), using a set of 397 shallow earthquakes distributed worldwide that occurred from 1987 to 1991, ranked earthquakes by energy and by moment. When earthquake size was ranked by energy, the list of the 20 largest events was dominated by strike-slip earthquakes (Table 3). When earthquake size was ranked by seismic moment, the list of the largest events was dominated by thrust-fault earthquakes. Two large strike-slip earthquakes off the western coast of the United States, for example, are ranked sixth and ninth by energy, but are ranked 36th and 55th by moment. Thus, if a criterion for seismic hazard is earthquake size, then it is important to note that the potential for damage predicted by energy and moment would be

different. A second feature in the comparison of rankings is that most of the large (high M_e) strike-slip earthquakes are associated with tsunamis. Although strike-slip earthquakes are not generally thought of as such, they may be capable of generating tsunamis. Thus, M_e may be useful in complementing M_W and M_S in evaluating tsunamic potential.

TABLE 3. Twenty largest earthquakes between 1986-1991 ranked by energy in terms of M_e. The corresponding M_S and M_W are also given. Three significant digits are used in M_e and M_W in order to refine the ranking. T indicates a tsunami was generated; a wave height, if reported, is also given. The type of faulting mechanism (FM) is indicated by TH (thrust), NR (normal) and SS (strike-slip).

Rank	Region	Date	FM	M_e	M_W	M_S
1.	Gulf of Alaska (T = 85 cm)	1987 11 30	SS	8.42	7.91	7.6
2.	Macquarie Islands (T)	1989 05 23	SS	8.12	8.10	8.2
3.	Gulf of Alaska (T = 10 cm)	1988 03 06	SS	8.12	7.79	7.6
4.	Gulf of Alaska (T = 10 cm)	1987 11 17	SS	7.74	7.21	6.9
5.	Luzon, Philippines	1990 07 16	SS	7.65	7.74	7.8
6.	Western Iran	1990 06 20	SS	7.49	7.43	7.7
7.	Coast N. Calif. (T = 50 cm)	1991 08 17	SS	7.39	7.10	7.1
8.	Aroe Islands (T)	1988 07 25	NR	7.35	6.96	6.7
9.	Tonga Islands (T = 25 cm)	1991 04 06	SS	7.22	6.69	6.7
10.	Mariana Islands (T = 24 cm)	1990 04 05	NR	7.23	7.47	7.5
11.	Tonga Islands	1987 10 06	NR	7.26	7.30	7.3
12.	Off Coast of Oregon	1991 07 13	SS	7.24	6.88	6.9
13.	Costa Rica (T = 2 m)	1991 04 22	TH	7.14	7.68	7.6
14.	Burma-China Border	1988 11 06	SS	7.13	7.05	7.3
15.	Banda Sea	1987 06 17	TH	7.03	7.12	--
16.	E. Papua New Guinea	1987 02 08	SS	7.04	7.36	7.4
17.	S. of Fiji	1989 08 14	SS	7.00	6.31	5.9
18.	Macquarie Islands	1990 09 17	SS	7.00	6.44	6.0
19.	Molucca Passage	1989 02 10	TH	6.99	7.15	6.8
20.	Coast of N. Chile(T=22 cm)	1987 03 05	TH	6.97	7.60	7.3

TABLE 4. Twenty largest earthquakes between 1986-1991 ranked by moment in terms of M_W. The corresponding M_e and M_s are also given. T indicates a tsunami was generated; a wave height, if reported, is also given. The type of faulting mechanism (FM) is indicated by TH (thrust), NR (normal) and SS (strike-slip).

Rank	Region	Date	FM	M_e	M_W	M_S
1.	Macquarie Islands (T)	1989 05 23	SS	8.12	8.10	8.2
2.	Gulf of Alaska (T=85 cm)	1987 11 30	SS	8.42	7.91	7.6
3.	Gulf of Alaska (T=10 cm)	1988 03 06	SS	8.12	7.79	7.6
4.	Luzon, Philippines	1990 07 16	SS	7.65	7.74	7.8
5.	Sulawesi	1990 04 18	TH	6.90	7.68	7.4
6.	Costa Rica (T=2 m)	1991 04 22	TH	7.14	7.68	7.6
7.	South of Fiji	1990 03 03	SS	6.95	7.65	7.4
8.	Kuril Islands	1991 12 22	TH	6.61	7.63	7.4
9	Coast of N. Chile (T=22 cm)	1987 03 05	TH	6.97	7.60	7.3
10.	Solomon Islands	1988 08 10	TH	6.50	7.60	7.4
11.	Mindanao, Philippines	1989 12 15	TH	6.64	7.59	7.3
12.	Sulawesi	1991 06 20	TH	6.45	7.57	7.0
13.	Mariana Islands (T=24 cm)	1990 04 05	NR	7.23	7.47	7.5
14.	Macquarie Islands	1987 09 03	NR	6.76	7.43	7.3
15.	E. Coast Honshu (T=56 cm)	1989 11 01	TH	6.85	7.43	7.4
16.	Western Iran	1990 06 20	SS	7.49	7.43	7.7
17.	New Britain (T=13 cm)	1987 10 16	TH	6.37	7.41	7.4
18.	Taiwan	1986 11 14	TH	6.94	7.41	7.8
19.	E. Papua New Guinea	1987 02 08	SS	7.04	7.36	7.4
20.	Costa Rica	1990 03 25	TH	6.36	7.36	7.0

Estimates of radiated energy for historical earthquakes

For earthquakes that predate the advent of broadband digital instrumentation, E_S can still be estimated if seismograms recorded by broadband instruments can be found and if such records are legible. However, unearthing such records and performing the digitization is both a challenging and daunting task. Fortunately, there may be an alternative. The preliminary results of Choy and Boatwright (1995) show that many seismic regions have a characteristic apparent stress, $\tau_c = \mu E_S / M_0$. Solving for E_S and inserting the expression into the definition of M_e,

$$M_e = 2/3 [\log M_0 + \log (\tau_c / \mu)] -2.9$$

This equation implies that M_e, as well as E_S, can be estimated for an historical earthquake in a given tectonic setting and a specific faulting type if the M_0 is known. In contrast to E_S, M_0 for historical earthquakes can be derived in numerous ways from geodetic and geologic methods, as well as the spatial distribution of aftershocks.

Conclusions:

Radiated seismic energy is a fundamental measure of earthquake size that is different from seismic moment. It can be used to complement seismic moment in evaluating seismic and tsunamic hazard.

- E_S can be directly computed from seismic data. It need not be an empirical quantity.
- Energy is physically different measure of earthquake size than moment. E_S is a better estimate of the potential for damage than M_0.
- M_e can be used to distinguish between earthquakes with identical M_W but different macroseismic effects.
- The correlation between E_S and M_0 varies systematically with faulting type, seismic region and tectonic environment.
- In particular, the energy radiated by intraslab normal-faulting earthquakes is a generally larger than that of interplate thrust-faulting earthquakes. For some normal-faulting intraslab earthquakes M_e is more effective than M_W in quantifying macroseismic effects.
- Oceanic strike-slip earthquakes can be followed by tsunamis. M_e may be a useful complement to M_W and M_S in evaluating tsunamic potential.
- As statistics about radiated energy and moment are accumulated, and their global variations become more precise, the seismic hazard potential can be estimated from historical as well as contemporary data.

REFERENCES

Boatwright, J., and G. L. Choy, Teleseismic estimates of the energy radiated by shallow earthquakes, *J. Geophys. Res.*, *91*, 2095-2112, 1986.

Choy, G. L., and J. L. Boatwright, Global patterns of radiated seismic energy and apparent stress, *J. Geophys. Res.*, *100*, 18205-18228, 1995.